

## Design, Optimization and Initial Testing of a High-Speed 5-kW Permanent Magnet Generator for Aerospace Application

Flur R. Ismagilov, Vyacheslav Ye. Vavilov\*, Aybulat H. Miniyarov, Aleksey M. Veselov, and Valentina V. Ayguzina

**Abstract**—The article presents a new topology of the high-speed synchronous electrical machines with permanent magnets with the tooth-coil windings with a stator magnetic core made of amorphous alloys for prospective unmanned aerial vehicles. This is a multidisciplinary design algorithm with optimization elements, which are proposed to design such machines. Based on the proposed algorithm, calculations of several topologies were performed by using computer simulation methods. In addition, the analysis of the rotor dynamics as part of the turbojet engine of the unmanned aerial vehicle and the calculations of the mechanical rotor strength were performed. To minimize the eddy-current losses in permanent magnets, the multicriteria optimization of the slotted zone was carried out by using genetic algorithms. A cooling system was proposed, and thermal calculations were performed. To verify the proposed design algorithm and to evaluate the efficiency of the amorphous alloy, a full-sized 5 kW experimental sample with a rotational speed of 60,000 rpm was created. Results can be used to create new promising UAVs and to design electrical machines for other industrial applications.

### 1. INTRODUCTION

A promising trend in the aerospace technology development is design and development of the unmanned aerial vehicles (UAVs). According to the investment agency estimates, the UAV market will be about 250 billion dollars by 2035 [1]. Up to 50% of this market will be occupied by UAVs with a turbojet engine (TJE) [1]. The main consumers of this market are both the defense industry and various commercial applications. The UAVs are actively used for monitoring and diagnostics of oil and gas pipelines, irrigation and watering of fields, for the delivery of goods, etc. Expansion of the tasks solved by UAVs and their functional purpose increases the power consumption requirements of their control and auxiliary systems. This requires an increase in the power of the electrical energy primary sources on the UAV board with a tendency to minimize the apparatus sizes [2]. A number of research teams are looking for a solution to this problem by using Li-Ion batteries [3], solar cells or piezoelements [4]. These concepts are still in the initial research state.

Therefore, even in the wide use conditions of the Li-Ion batteries, the main electrical energy source on the UAV board is electrical machines, which should provide simultaneous launch of turbojet UAVs and provide all UAV systems with electrical energy. Thus, to create promising UAVs with a turbojet engine, high-efficiency starter-generators (SG) are required. In addition to UAVs with a turbojet engine, the tasks of creating high-efficiency SGs are also in the UAVs on electric traction. Now the main direction of their development is the use of hybrid schemes, where the SG is the main energy source for the traction motor and largely determines the UAV capabilities, flight time and its speed characteristics [5–9].

---

*Received 18 September 2017, Accepted 4 November 2017, Scheduled 30 November 2017*

\* Corresponding author: Vyacheslav Evgenievich Vavilov (s2.88@mail.ru,vavilovv@ugatu.su).

The authors are with the Department of Electromechanics, Ufa State Aviation Technical University 12 K. Marx Street, Ufa 450008, Russian Federation.

The main SG requirements are the maximum energy density per unit mass, minimum weight-and-size parameters and the possibility of direct connection without a gearbox with a high-speed shaft of a turbojet engine (high-speed shaft speed is 48000–96000 rpm).

The development prospect of the UAV turbojet engine and its SG is the realization of them by oil-free dry technology on magnetic or gas bearings. There are already a number of turbojet engine models on the gas bearings. A serious limitation in the UAV design is the failure of the liquid cooling system and the use of only air-cooling. These requirements are related to the prospects for introducing non-lubricating technologies in the turbojet engine. In addition, the SG of the UAV does not have its own bearings. It is installed on the shaft of the turbojet engine, which complicates the requirements for the rotor dynamics calculations, since it should be calculated together with the rotor of the turbojet engine. All these requirements can be effectively realized with the high-speed synchronous electrical machines with permanent magnets (HSPMs) and tooth-coil windings (HSPMTC) [6]. Advantages of HSPMTC are the absence of the need of the excitation power, the maximum energy density and efficiency, which is above 96%, the minimum overall dimensions of the winding frontal parts due to the use of the tooth-coil windings and, accordingly, the reduced rotor length, which has a positive effect on the entire rotor dynamics of the turbojet engine.

In [6–8] it is shown that HSPMs with an external rotor are better than with an inner rotor due to their high power density. However, it is difficult to integrate such machines on the shaft.

Therefore, this paper describes and explores a new topology of the 5 kW HSPM with the inner rotor, a rotational speed of 60,000 rpm and specific characteristics of 0.20 kg/kW for UAVs. The topology novelty is in the use of amorphous alloys as a stator material, which allows achieving an efficiency over 96%.

The first section of the paper is devoted to the global trend review of the HSPM for UAVs and evaluation of the results achieved. It is shown that achieving an energy density of 0.2–0.25 kg/kW in a low-powered HSPM is a complex, nontrivial task with no commercial solutions. The second section describes the approach to the HSPM design. It gives the computer simulation results of the rotor dynamics and HSPM electromagnetic fields. It is also shown that to achieve the desired power density and efficiency, the design process should include not only multidisciplinary calculations, but also elements of optimization calculations. The third section describes the experimental layout and test results.

## 2. RESEARCH LANDSCAPE

The HSPMs with power of 1–5 kW and a 48,000-rpm rotational speed and above are widely used in various industries: machine tools, medicine, microturbine plants, etc. [10]. There are a number of commercial solutions in this power range [11–14]. Nevertheless, in view of their general industrial orientation, no decisions can be used in the UAVs, as HSPMs for the UAVs are usually created as an element of a turbojet engine. Therefore, it seems advisable to consider only commercial solutions created specifically for the UAVs.

PBS Velká Bíteš produces the TJ-100 turbojet engine, in which a 0.7 kW HSPMTC with a 60,000 rpm rotational speed is integrated [15]. In the TJ-50 and TJ-120 turbojet engines by Hamilton Sundstrand, the HSPMs with rotational speed of 60,000–150,000 rpm are used [16]. The AN/USD-502 reconnaissance aircraft uses the 4 kW HSPM with a rotational speed of 60,000 rpm [17]. In most serial and advanced UAVs, the HSPMs are used with a rotational speed of 60,000 rpm and a power of up to 5 kW. The SG rotational speed limitation is due not to the SG characteristics, but to the turbojet engine characteristics. In investigated SG, the rotational speed of the turbojet engine is 60,000 rpm.

The power HSPM limitation at 5 kW of modern UAV is due to the limited power and volume of turbojet engines, because the mechanical power for the HSPM electrical energy generating is taken from the turbojet engine shaft. The turbojet engine volume determines practically all the UAV dimensions. The increase in the SG power density allows a decrease in the SG volume and, accordingly, the increase in the turbojet engine volume with the same dimensions of the UAV. This will ensure an increase in the UAV flight time, its speed and payload.

Therefore, the increase in the UAV power density is an important task. This also largely determines the tactical and technical characteristics of the UAV.

Prospective HSPMs with a power of 100–300 kW for manned aircraft already reach power density of 0.1–0.15 kg/kW. For example, Borg Bartolo et al. describe starter-generators with these parameters [18]. Siemens describes an electrical motor for aerospace applications with a 0.15 kg/kW power density [19]. Similar solutions are described in the works of Ganev [20, 21]. Thus, the energy density of the high-power aviation HSPM has already reached very good results [18–21]. However, at the same time, the HSPM energy density of small and medium power decreases with the power decreasing, even with a significant increase in the rotor rotational speed and in the cooling efficiency. For example, the HSPMs with the highest speed in the world produced by Celeroton have a mass of 36 grams and, respectively, the power density of 0.36 kg/kW at a 500,000–800,000 rpm rotational speed and a 55–100 W power.

Similar problems occur with the efficiency, because with reduced power, the efficiency of the HSPM with small and medium power is also reduced. Figure 1 shows the obtained curve, which characterizes the decrease in the power density and efficiency as a power change function. The curve is based on the analysis of promising developments and industrially produced HSPM of the aviation systems [6–23].

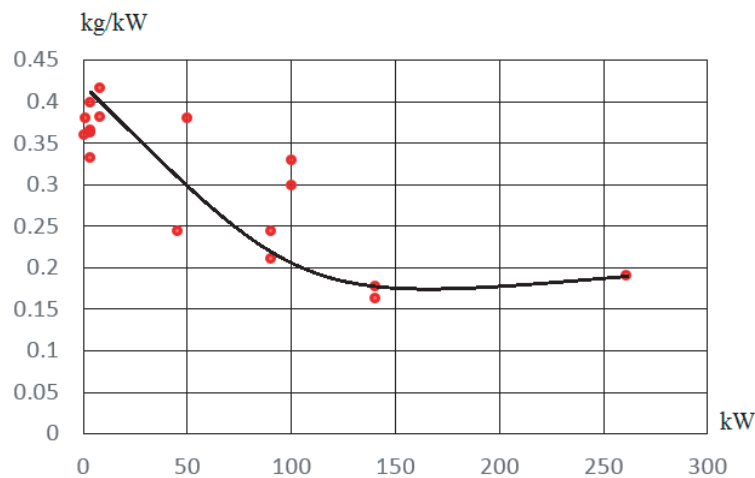


**Figure 1.** Energy density dependence of the aerospace SG on power.

Figure 1 shows that the minimum achieved energy density of commercial high-speed SG of the UAVs is 0.32–0.33 kg/kW at the power below 5 kW. Thus, the requirements for the SG power density are not achieved by commercial solutions. This proves that the design of the 5 kW HSPM with a 48,000–96,000 rpm rotational speed, specific mass of 0.2 kg/kW or below, and with efficiency over 96% is a nontrivial, complex scientific and technical task.

This task involves a number of technical problems, some of which are typical for all HSPMs, and some are only for UAVs.

1) Loss problems due to the high magnetization reversal frequency of the stator core. To solve it, the amorphous alloy is used in the proposed topology. This allows the steel loss minimization by 400–600% in comparison with the silicon or cobalt alloys. Research works on the design of electrical machines with a stator core made of amorphous alloy are presented in [22–24]. Nevertheless, the industrial SG designs for UAVs are not presented. In this paper, the topology with a stator core made of amorphous alloy is described, and its investigations are presented.

2) Problems caused by eddy-current losses in permanent magnets. To achieve the minimum overall dimensions, the tooth-coiled windings should be used. This will lead to the appearance of the magnetomotive force spatial harmonics and the eddy currents in the permanent magnets of the HSPM. To minimize these losses, the multicriteria optimization of the HSPM slot zone was made. Losses in permanent magnets are reduced by 2–2.5 times.

3) Problems caused by the SG integration into the turbojet engine. One of the main task is to provide the subcritical rotor dynamics of HSPM in conjunction with the turbojet engine. In addition, the HSPM thermal state requires detailed analysis due to air-cooling. Therefore, in this article, the HSPM rotor dynamics in conjunction with the turbojet engine is analyzed, and the cooling system is

optimized. There are also problems with ensuring the rotor mechanical strength, which are considered in [11–14].

As a research result, a full-size sample with a tooth-coiled windings and stator core made of amorphous alloy is created. The article presents the test results at low rotational speeds. This proves the correctness of technical solutions. Herewith, power density of the created sample is 0.2 kg/kW.

### 3. MACHINE DESIGN AND OPTIMIZATION

The main novelty and difficulty in implementing the proposed topology of the HSPMTC is the use of amorphous alloy. The HSPMTC design was carried out based on these features. Therefore, the following HSPMTC topology selection algorithm was used:

Step 1. From the technological possibilities of the amorphous alloy, the number of stator slots was determined. The HSPMTC cooling scheme and slot number are fixed. For the selected slot number, the rotor materials were selected, and preliminary electromagnetic calculations were performed for all possible variants of the rotor pole number. In this case, the rotor geometric dimensions, which remained the same for any pole number in subsequent iterative calculations, were determined. Calculations of winding data and mechanical calculations of the rotor were also performed. Several topologies were compared, and the optimal pole number was selected.

Step 2. Since the rotor geometric dimensions are assumed as fixed for any pole number, the further rotor dynamics analysis of the HSPMTC in conjunction with the turbojet engine shaft was carried out. In case of unsatisfactory results, step 1 should be repeated, and the new rotor geometric dimensions should be selected. In the case of satisfactory results, it is necessary to continue the HSPMTC designing.

Step 3. Optimization of the HSPMTC slot zone and the dimensions of the ferromagnetic slot wedge is performed by the minimal loss criterion. Loss calculations were performed for the selected optimal values. Optimization tasks are solved by using genetic algorithms implemented in commercial software products.

Step 4. HSPMTC thermal calculations. In the case of unsatisfactory results, correction should be made in step 3 or, if the technological capabilities permit, the cooling system optimization. In case of satisfactory results, a prototype is created.

The proposed algorithm differs from the known HSPM design methodologies [25–27]. The main difference is the selection and fixing of the slot number, as well as the cooling system and the restriction absence of the pole number. These differences are due to technological features of the amorphous alloy use. Typically, high-speed electrical machines have one pole pair to minimize losses in the stator core.

However, since the magnetic core is made of amorphous alloy, which has low specific eddy-current and hysteresis losses, a large pole number can be used in the studied topology. It is limited by the number of stator slots, i.e., the possibility of implementing a winding scheme for a certain slot number per pole and phase. In other aspects, the proposed algorithm is similar to an established calculation sequence [25–27].

Step 1. To use amorphous alloy in the HSPMTC stator, the following approach is proposed. From the amorphous alloy tape, several triangular magnetic cores are formed. The number of triangular magnetic cores corresponds to the number of HSPMTC stator slots. It is important to notice that this slot number should be minimal to reduce the economic costs of production. Figure 2 shows experimentally created magnetic cores from amorphous alloy for the projected HSPMTC.

One of the important advantages of magnetic cores according to the proposed technology is technological channels for the HSPMTC cooling, which are formed during production. They are presented in Figure 3. These channels significantly improve the heat dissipation from the HSPMTC active zone. The air moves in three ways: in the stator body, along the air gap and over the stator surface.

The HSPMTC with a stator core without a stator back (Figure 2(a)) has only 2 cooling channels. To minimize windage losses in the air gap between the stator and the rotor, a ceramic sleeve was installed. To reduce economic costs in the HSPMTC production with a magnetic core made of amorphous alloy, it is necessary to select the minimum slot number. Therefore, the HSPMTC was performed with a slot number equal to 6. The stator was made of 5BDSR amorphous alloy with a 1.35 T saturation magnetic flux density and specific losses below 5 W/kg at a 1000 Hz frequency and a 1.25 T magnetic flux density.

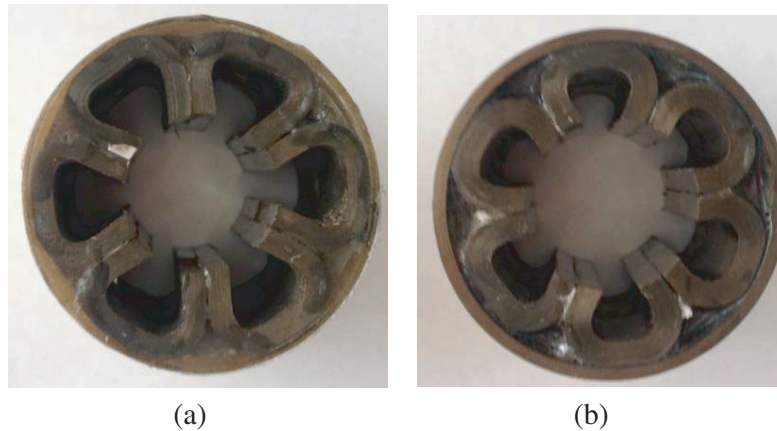


**Figure 2.** Magnetic cores made of amorphous alloy by the proposed technology: (a) without a stator back; (b) with a stator back.

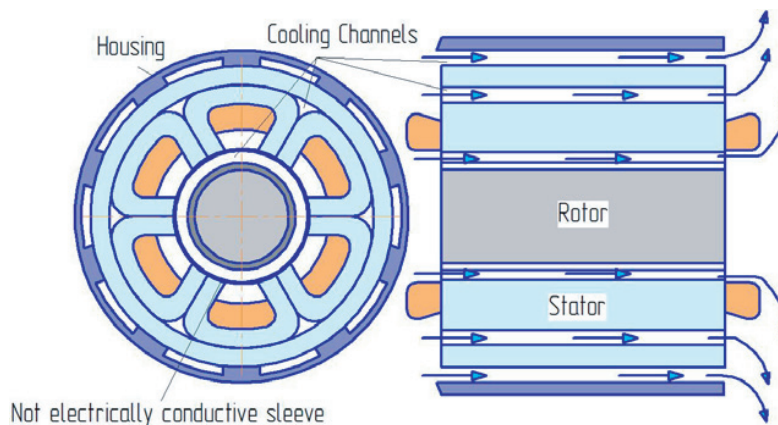


**Figure 3.** The HSPMTC cooling system.

The HSPMTC windings were tooth-coiled from a Litz with a strand cross-section of  $1.13 \text{ mm}^2$ . The strand number was 30 in the slot, and 15 in each coil. The current density in the designed HSPMTC was below  $6\text{--}8 \text{ A/mm}^2$  before the optimization calculations. The wire insulation was polyimide with temperature index of  $220^\circ\text{C}$ . In addition, to minimize the harmonics created by the spatial magnetomotive force, a ferromagnetic slot wedge was used. The wedge dimensions are optimized in the next stage. Figure 4 shows the structural diagram of the stator magnetic core of the designed HSPMTC. In the HSPMTC development, two structural stator designs created according to the proposed topology were considered: a magnetic core formed from a tape with a 50 mm length and a magnetic core from several cores with a 5 mm length. It is obvious that the first magnetic core is simpler due to the technological capabilities, and the second should have lower eddy-current and hysteresis losses.

The stator magnetic core dimensions were selected so that the magnetic flux density in the teeth and the stator back were the same. In this case, the specific losses in the teeth and back will be the same. The total losses in the stator core will depend on the stator teeth and stator back masses.

In HSPMTC with a distributed winding and stator magnetic core made of electrical steel, it is difficult to achieve the same mass of teeth and back. Therefore, the loss distribution along the stator magnetic core is almost always uneven.

For a bipolar HSPMTC with a stamped stator magnetic core, the stator back losses are higher than the stator teeth losses.

In HSPMTC created according to the proposed technology, the stator back is formed separately from the teeth. This allows to achieve approximately the same mass of the back and teeth. The

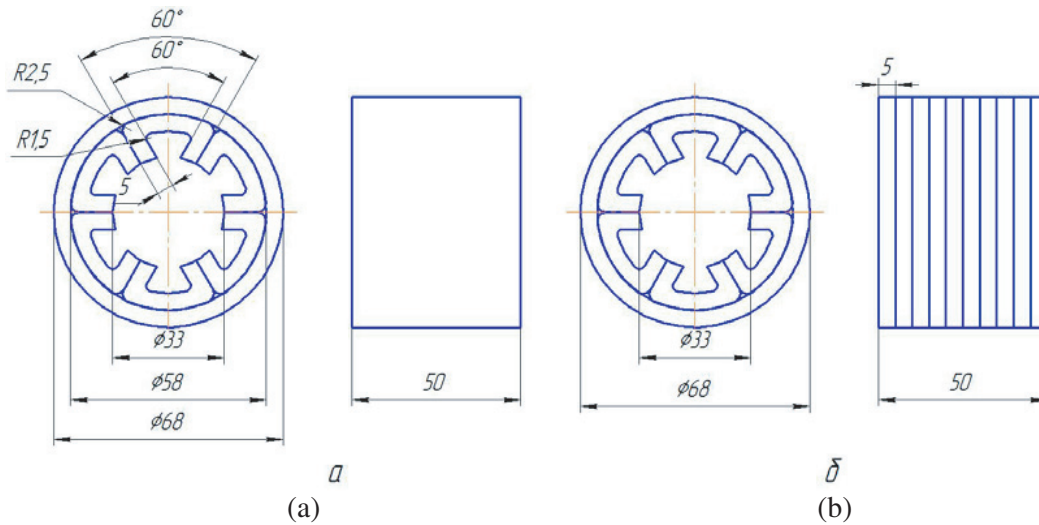


**Figure 4.** Geometric dimensions of the investigated stator topologies: (a) from a tape with a 50 mm length; (b) from several cores with a 5 mm length.

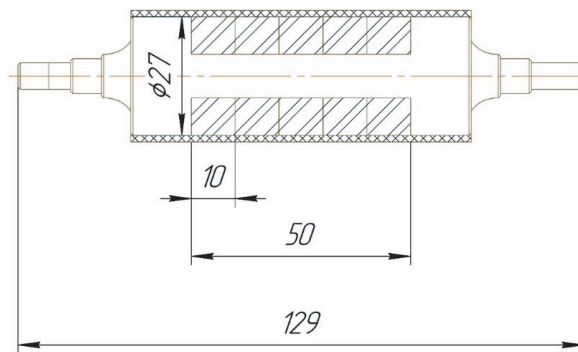


**Figure 5.** Geometrical dimensions and design diagram of the HSPMTC rotor.

difference between these masses is below 20–30%. Thus, the statorcore loss distribution is practically uniform.

Taking into account the stator geometric dimensions, the rotor dimensions of the designed HSPMTC were calculated. It was made of SmCo permanent magnets ( $B_r = 1.07$  T;  $H_c = 756$  kA/m). The rotor diameter was 28 mm; the axial length was 50 mm. To ensure the rotor mechanical strength, a carbon fiber sleeve with a thickness of 1.5 mm was installed over the permanent magnets. A carbon fiber was selected because it has a sufficient mechanical strength and provides minimal eddy-current losses. This is due to the manufacture technology: the carbon fiber winding and the epoxy impregnation. Thus, the eddy-current circuit in the carbon fiber bandage is minimal.

For integral bandages of titanium or Inconel, the eddy-current circuit is large, which significantly increases the losses. At the preliminary calculation stage, the four-pole and two-pole HSPMTC topologies were considered. Figure 5 shows the rotor design diagram with the dimensions obtained in the preliminary calculation results.

Typically, high-speed electrical machines use 2 poles to minimize losses in the stator core. Nevertheless, since the amorphous alloy has a low specific losses, a large pole number can be used in the proposed topology.

The pole number is limited by the stator slot number. As shown above, 6 slots are used. Therefore, to implement the tooth-coiled winding, either 2 or 4 poles can be used. The slot number per pole and phase are 1/2 and 1. Table 1 shows the preliminary calculation results for the 2-pole and 4-pole HSPMTC topologies.

**Table 1.** The preliminary calculation results for the 2-pole and 4-pole HSPMTC topologies.

Parameters	Value	
	2-pole HSPMTC	4-pole HSPMTC
Power, [kW]	5	5
Number of stator slots	6	6
Rotor rotational speed, [rpm]	60000	60000
Operating phase voltage, [V]	115	115
Current density, [A/mm <sup>2</sup> ]	12	7
Number of turns in phase	58	30
Active stator length, [mm]	48	48
Outer stator diameter, [mm]	68	58
Rotor magnet diameter, [mm]	28	28
Rotor bandage diameter, [mm]	31	31
Material type	5BDSR with thickness of 25 microns	
Saturation magnetic flux density, [T]	1.35	1.35
Permanent magnet type, $B_r$ , [T]/ $H_c$ , [kA/m]	SmCo, 1.07/756	SmCo, 1.07/756
Bandage thickness, [mm]	4	4
Bandage material	Carbon	Carbon
Bandage material strength, [MPa]	1500	1500
Mass of active parts, [kg]	1	0.8
Stator length including frontal parts, [mm]	60	60
Coolant	Air	Air

Figure 6 shows the computer simulation results of electromagnetic fields in these topologies. The computer simulation was performed taking into account the nominal load.

Computer simulation results show that the 4-pole magnetic system allows to achieve lower mass- and size parameters due to the lack of the outer ring of the magnetic core made of amorphous alloy (Figure 2(a)).

The mass of this ring is 200 grams (50% of the stator magnetic core mass). The magnetic flux density in the stator magnetic core with a 4-pole magnetic system is 1.2 T, and the permanent magnet losses are  $3 \cdot 10^8$  W/m<sup>3</sup>.

At this stage, a rotor made of a permanent magnet with 50 mm length was considered. At the optimization stage, the variants of performing a rotor with several permanent magnets located one after another in the axial direction were considered.

For the equal output voltage in topologies, the turn number, current density and losses in the winding in 4-poles HSPMTC are less than that for the 2-poles HSPMTC.

The significant drawback of the 4-pole magnetic system is the high magnetization reversal frequency of the stator (2000 Hz) and the resulting eddy-current and hysteresis losses in the stator magnetic core. For a 2-pole magnetic system, the magnetization reversal frequency of the stator is 1000 Hz. The magnetic flux density in the stator core is 1.5 T. This value is higher than the saturation magnetic flux density of the 5BDSR amorphous alloy. The stator core mass is 400 grams. The eddy-current and hysteresis losses in permanent magnets of the 2-pole magnetic system are  $2.1 \cdot 10^8$  W/m<sup>3</sup>. This value is less than that for the 4-pole magnetic system by 30%.

It is obvious that the 100% increase in the magnetization reversal frequency between the 2-pole and 4-pole magnetic systems will lead to an increase in the eddy-current stator core losses of the 4-pole HSPMTC by 300% in the first approximation. However, the total losses of the 4-pole rotor will be higher than that for the 2-pole rotor by 50%, since the stator magnetic core mass of the 2-pole HSPMTC is higher by 100%, and the magnetic flux density is higher by 20%. The losses are determined by the



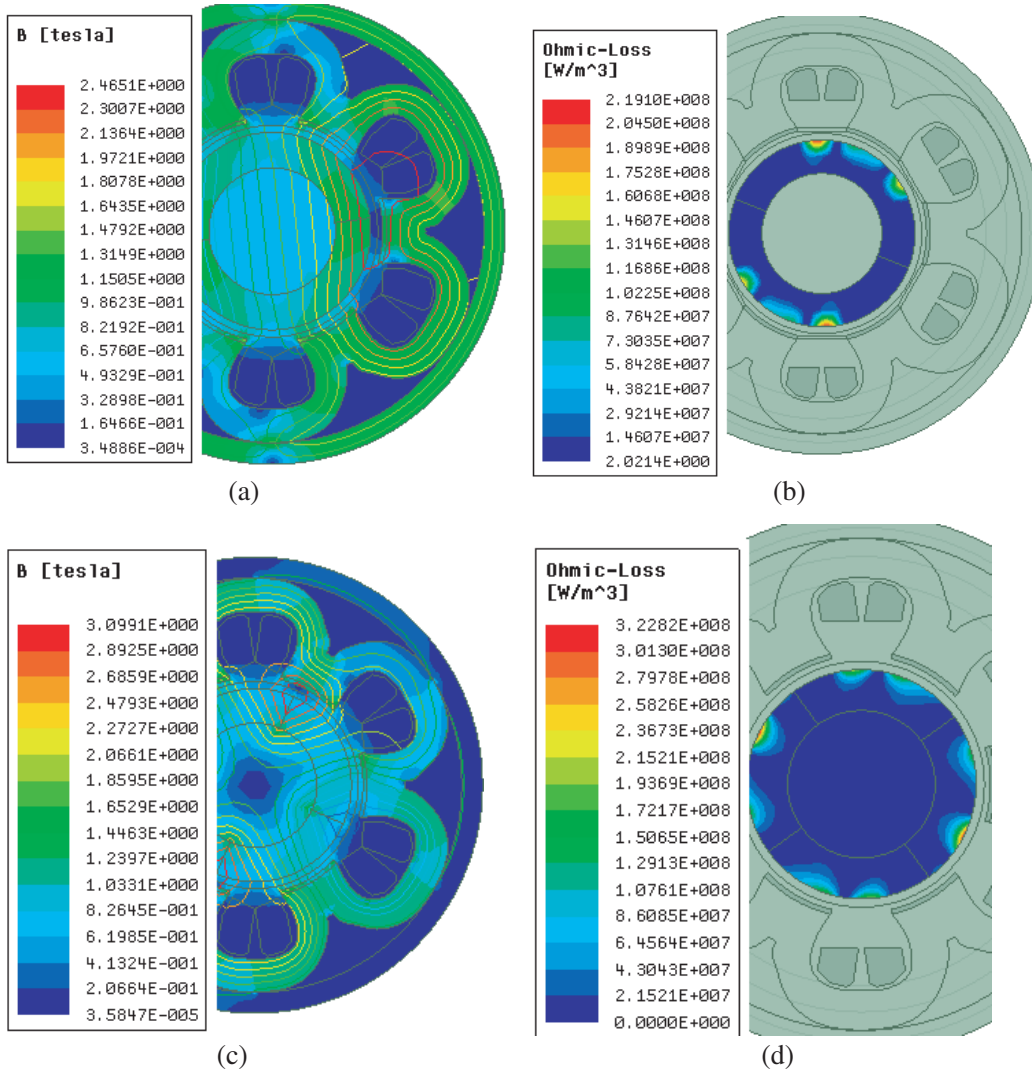


**Figure 6.** Computer simulation results of HSPMTC: (a) the magnetic flux density in the 2-pole HSPMTC; (b) eddy-currents losses in permanent magnets in the 2-pole HSPMTC; (c) the magnetic flux density in the 4-pole HSPMTC; (d) eddy-currents losses in permanent magnets in the 4-pole HSPMTC.

stator magnetic core mass, magnetic flux density and frequency.

For the stator core made of amorphous alloy, the losses will not exceed 7 W at 2000 Hz frequency and 1.2 T magnetic flux density. For the 2-pole topology, these losses will be 4.6 W. This conclusion will be proved experimentally.

The winding losses of the 4-pole topology (22 W) are lower than for the 2-pole topology (62.5 W). Therefore, the 4-pole HSPMTC topology was selected. The total stator core losses of this topology are 29 W, and for the 2-pole topology the total stator core losses are over 60 W.

The result obtained differs from the results of the well-known works [25–27], where the 2-pole topology is recommended. This difference is due to the use of amorphous alloy. The disadvantage of the 4-pole topology is the high eddy-current losses in permanent magnets. Therefore, after the rotor critical speed calculations, the slot zone optimizing problem is solved, and the most effective thickness of the permanent magnet sector is selected by the minimum loss criterion.

Next, variants of the rotor from the set of permanent magnets are considered.

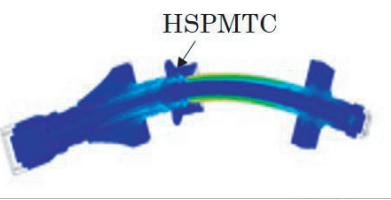
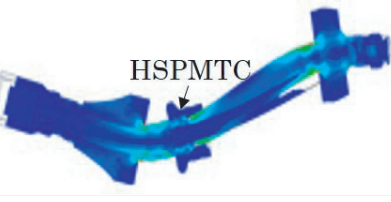
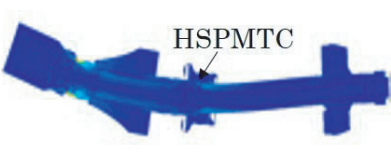
Step 2. After determining the pole number, the geometric dimensions of the HSPMTC active part, an analysis of the rotor dynamics is performed. Since HSPMTC is integrated into the turbojet engine,



its rotor dynamics should be considered in conjunction with the dynamics of the turbojet engine rotor. Otherwise, calculating only the rotor dynamics of the electrical machine will lead to the turbojet engine destruction risk after installing an electrical machine on its shaft. In general, this feature applies to all integrated electrical machines.

To calculate the rotor dynamics and to analyze the forces acting on the rotor, the finite element method was used by using the Ansys Maxwell software package. Table 2 shows the rotor dynamics calculation results for the turbojet UAV with the installed HSPMTC.

**Table 2.** The HSPMTC losses.

Critical speed	Model	Rotational speed (percent age of the nominal), [rpm]
First critical speed		17,700 (30.0%)
Second critical speed		41,400 (70.2%)
Third critical speed		70,600 (119.7%)

Based on the simulation results, the critical speed margin for the SG is above 20% of the first critical speed value.

The rotor dynamics analysis results show that the third critical speed is higher than the nominal speed by 117%. At the speeds close to 60,000 rpm, no critical speeds are observed. Therefore, the obtained results are considered as positive. This allows proceeding to the next step: the slot zone optimization and the loss determination in the HSPMTC.

Step 3. From the results of the two previous steps, it can be seen that the projected HSPMTC at this stage in the energy density terms corresponds to the set conditions. The mass of its active part is 0.8 kg at 5 kW power. Taking into account the housing mass, the power density of the developed HSPMTC is 0.2 kg/kW. Since HSPMTC is integrated into the turbojet engine, it does not have its own bearing shields and bearings. Bearings are only required for the HSPMTC testing and are not taken into account for the calculation mass.

However, the problem of the developed topology remains high eddy-current losses in permanent magnets. In conditions of difficult heat removal from the rotor, these losses can lead to overheating of permanent magnets and failure of the entire SG. In [10–22], to determine the losses in permanent magnets, their crushing in the axial direction is used. The preliminary calculations show that the loss reduction is approximately 150–200% by crushing the permanent magnets from the one sector length of 50 mm to the one sector axial length of 5 mm.

Obviously, this is not enough to achieve the maximum HSPMTC efficiency, since the HSPMTC will be operated in conjunction with the rectifier. Consequently, losses in permanent magnets will also be caused by the time harmonics. Therefore, it was decided to optimize the HSPMTC slot zone by minimizing the eddy-current losses in permanent magnets due to the ferromagnetic wedge from the

Magnoval 2067 material. The slot dimensions stayed unchanged because of the technological limitations in the stator magnetic core formation from amorphous alloy.

With the same slot sizes, the use of a ferromagnetic wedge will lead to an increase in the winding losses and the current density. Thus, the task of multicriteria optimization arises.

This task is solved by using the genetic algorithms implemented in the Ansys Maxwell software package. Two input variables were considered: the height of the ferromagnetic wedge and the axial length of the permanent magnet sector. The initial population included 30 individuals, which had the same geometric dimensions and differed only in the height of the slot wedge, the axial length of the permanent magnet sector, and the number of sectors. The total lengths of permanent magnets for all individuals were the same. The output variables were the current density and eddy-current losses in permanent magnets. The population was multiplied by panmixia. The next population included 30 individuals. The selection was based on the Roulette method. The estimated optimization time did not exceed 1 hour. The optimization results are shown in Figure 8(a), where  $b$  is the ferromagnetic wedge height;  $j$  is the current density;  $P_{pm}$  is the eddy-current losses in the permanent magnets.

Based on the Pareto approach, the optimal ferromagnetic wedge height is 2.5 mm. Herewith, the eddy-current losses in permanent magnets are reduced by 75%. The current density and copper losses are increased by 20%.

Further increase in the slot wedge height results in a slight decrease in losses, but the current density and copper losses are increased linearly. With an increase in the slot wedge height to 3.9 mm, the eddy-current losses in permanent magnets are decreased by only 84%, but the current density in the windings and losses in the winding are increased by 45%. Thus, the 2.5 mm ferromagnetic wedge height is optimal for the studied topology and geometric dimensions. At this height, the principle of crushing permanent magnets in the axial direction was considered. Results are presented in Figure 7(b), where  $l_{pm}$  is the length of one permanent magnet. Figure 7 shows that the use of permanent magnets with a 10 mm axial length allows to reduce additional 130% of the eddy-current losses. Performing an even shorter length of permanent magnets is not advisable, since this will lead to a technological complication in the rotor manufacture, but it will not yield a significant gain in minimizing losses.

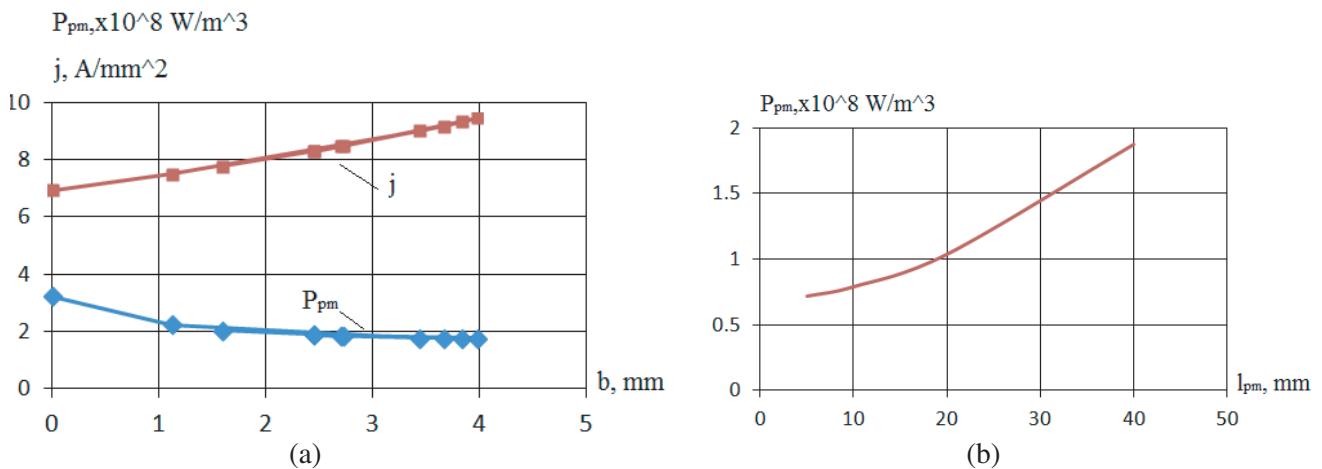


**Figure 7.** The HSPMTC optimization results by the criterion of minimum eddy-current losses in permanent magnets.

Thus, the optimization carried out at the design stage made it possible to reduce the eddy-current losses in permanent magnets by 300%.

After that, the total losses in all HSPMTC elements were calculated. The calculation results are presented in Table 3. Losses in bearings are not taken into account, because HSPMTC is integrated into the turbojet engine and does not have its own bearings.

Thus, the efficiency obtained from optimization and calculations with mechanical losses is 96.4%. This is a good result for the HSPMTC in the specified power range, because the HSPMTC with a 60,000 rpm rotational speed, 0.2 kg/kW energy density and efficiency of 96.4% for UAVs was obtained

**Table 3.** The HSPMTC losses.

The loss type	Loss dependence	Value
Windage losses	$P_w = c_f \pi \rho_{air} \Omega^3 D_b^4 l / 16$ , where $f$ is the air friction coefficient of the rotor; $\rho_{air}$ is the air density; $D_b$ is the rotor diameter; $\Omega$ is the rotation frequency [rad/s]; $l$ is the length of the part on which the losses are defined	$P_w = 125$ W
Losses in the winding	$P_{cu} = m I^2 R$ , where $m$ is the phase number; $I$ is the current; $R$ is the resistance	$P_{cu} = 27$ W
Stator core losses	Specific losses in amorphous alloy are 35 W/kg at a 2000 Hz frequency and a 1.2 T magnetic flux density	$P_s = 7$ W
Eddy-current losses in the rotor bandage and permanent magnets	It is determined by computer modelling in the Ansys Maxwell software package	$P_{ec} = 12$ W
Additional loss	Losses on eddy currents and proximity effect in the stator winding, the magnetization reversal losses of the stator core by a non-sinusoidal magnetic flux, additional losses in the frontal parts	$P_a = 15$ W
Total efficiency	$\eta = \frac{P}{P + P_w + P_{cu} + P_s + P_{ec} + P_a} \cdot 100\%$	96.4 %

in the result of the proposed technical solutions and optimization methods.

Step 4. The HSPMTC cooling system was described above. At this stage, only verification calculations were carried out. Herewith, verification calculations were carried out for the SG together with the turbojet engine. The SG cooling is supposed to be carried out by air from the impeller, which is then discharged into the channel of the central coupling bolt.

Figure 8 shows the design of the turbojet engine with the integrated SG, and paths of the cooling air movement throughout the turbojet engine. To minimize losses, the pole of the SG was laminated in an axial direction and was made of several sectors. Since the 4-pole topology was selected, there is no additional cooling channel in the SG formed by the stator back. The air moves only along two paths through the air gap between the stator and the rotor, and along the stator back. The maximum air temperature at the SG entrance was assumed to be +50°C. The air speed is 30 m/s. The temperature calculated in the AnsysIcePack did not exceed 80°C for permanent magnets, 130°C for the winding temperature and 108°C for the stator magnetic core. These temperature values do not exceed the established limits.

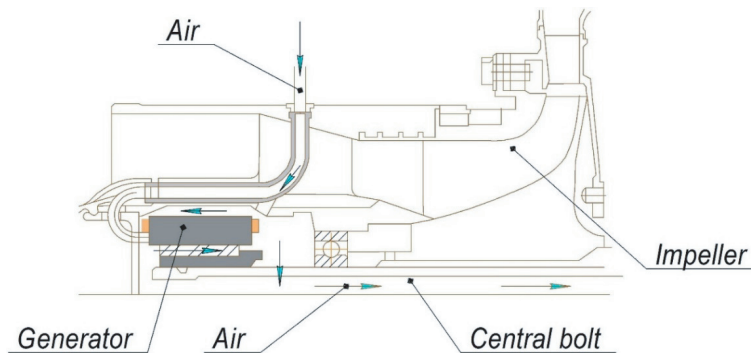


**Figure 8.** The SG cooling in the turbojet engine.

The heat calculation results confirm the HSPMTC operability. Based on the obtained results, the HSPMTC prototype samples were created, and their initial tests were performed.

#### 4. EXPERIMENTAL SAMPLES AND INITIAL TESTING

For experimental studies, two full-size experimental HSPMTC samples with 2-pole and 4-pole magnetic systems were created. Both samples have the geometric dimensions according to Table 1. Figure 9 shows the experimental sample of the 4-pole HSPMTC with the test layout.

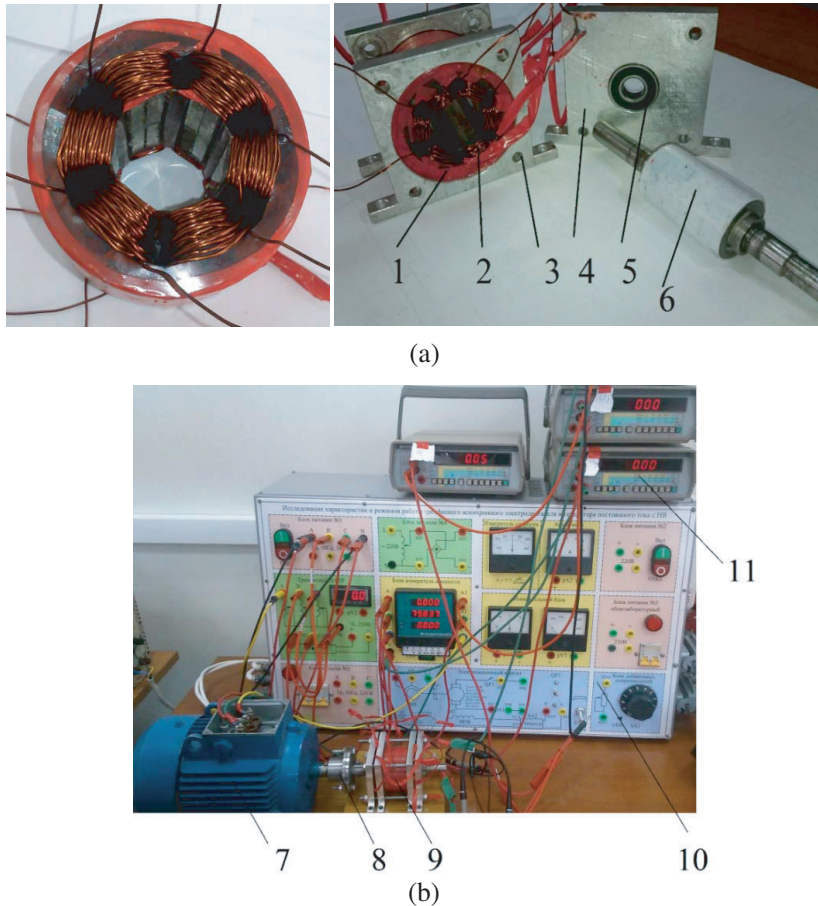


**Figure 9.** The experimental (a) HSPMTC sample and (b) measuring layout: 1 — stator core; 2 — tooth-coiled windings; 3 — mounting; 4 — bearing support; 5 — bearing ; 6 — rotor; 7 — drive motor; 8 — coupling; 9 — the experimental HSPMTC sample; 10 — test unit; 11 — measuring device.

The initial tests were performed at a reduced rotational speed. It was 3000 rpm for the 2-pole topology and 1500 rpm for the 4-pole topology. Two different rotational speeds were used to ensure the equal voltage frequencies of both generators. The results of experimental studies differ from computer simulation data below 3%. During tests, the SKF 638/8-2Z bearings with a maximum speed of 90,000 rpm were used. In addition, experimental studies were carried out at the increased rotational speed. In this case, the losses increase. However, the difference between the theoretical and experimental data was below 7%.

The main testing task was to assess the HSPMTC efficiency, which was carried out by direct measurements by the power consumption estimation of the drive (asynchronous motor) and the output power estimation of the sample during the testing in the generator mode. Next, the HSPMTC loss estimation methodology is described.

The HSPMTC efficiency evaluation in the generator mode was carried out for the more accurate measurements and a simple estimation of the windage losses in the sample. For this, two rotors of the same materials with the same surface treatment were made. One rotor was made with permanent magnets and the other without it. At the start-up of the layout drive with the permanent magnet rotor without a load, the consumed power was 81.5 W. At a start-up of the drive with coupling, without connection to the HSPMTC, the consumed power was 60 W.

In the generator mode without a load, only the windage losses, hysteresis and eddy-current losses in the stator, and losses in bearings occur in the created layout.

The next step is the power consumption measurement of the HSPMTC drive with a rotor without permanent magnets. The drive was a 1.5 kW asynchronous electrical motor with a rotational speed of 2800 rpm. The energy consumption of the induction motor was estimated by using the power analyzer Prizma-50. At the start-up of the HSPMTC layout with a rotor without permanent magnets, the drive's power consumption was 80 W per phase. In this case, only windage losses and losses in the bearings (i.e., mechanical losses) occur in the HSPMTC. It is obvious that the stator magnetic core losses in the 2-pole topology are 4.5 W.

For 10 minutes of the 2-pole HSPMTC sample operation, the stator magnetic core was heated to 60°C at this loss value. Taking into account the stator core mass, the specific losses are 11.25 W/kg. This loss value is quite large for a 50 Hz frequency. Therefore, a number of additional studies were carried out to elucidate such a large loss value. Losses in the stator magnetic core are estimated at a certain value of the magnetic flux density in the teeth, since the windings are tooth-coiled in the developed sample, and all flow passing through it will be the flow through the stator tooth. To estimate the magnetic flux density in the stator teeth, a fluxmeter was connected to the terminals of one coil. It was found that the magnetic flux density in the stator teeth is 1.5 T for the 2-pole topology and 1.22 T for the 4-pole topology. These data are in good agreement with computer simulation data and show the reason of the loss in the 2-pole topology. This is a significant saturation of the stator magnetic core, which is also indicated by the voltage oscillograms obtained in Figure 10.

For the 5BDS Ramorphous alloy, the saturation magnetic flux density is 1.35 T. For a saturated magnetic core, the loss estimation is not allowed, since in this case losses increase significantly in comparison with normal operating conditions. For the 4-pole topology, these problems were not present, which again confirms the correctness of the selected pole number.

The effective phase voltage value in the SG layout is 4.39 V at a 50 Hz frequency. With increase in the frequency by 40 times, the phase voltage is 118 V. This value corresponds to the computer simulation data. The sample mass is 1 kg taking into account the bearing shields, housing and bearings. The power density is 0.2 kg/kW.

The next step was to estimate the losses in the stator magnetic core at high magnetization reversal frequencies and at magnetic flux density values below saturation magnetic flux density. For this purpose, a 10-pole rotor was installed in the created magnetic core. Also the magnetic flux density was measured, which was 0.4 T, and the stator magnetic core losses, which were 0.3 W/kg. Within 10 minutes of operation, the stator temperature has been changed by 0.8°C, and the temperature of the stator teeth has been changed by 1°C. The stator back temperature was measured by the ThermoScopeTesto 870, and the teeth temperature was measured by the thermocouple installed on their surface.

The obtained values of specific losses in amorphous alloy are lower than the analogous values for electrical steel by 400–600%. Thus, the results of experimental studies confirm theoretical conclusions. It is important to notice that the stator packages of 5 mm in length is the most effective option to implement the proposed technology. This will further minimize losses. Now, together with our industrial partner, we have worked out the manufacturing technology of such a stator. In the following researches, it is planned to test this topology.

Since the researched HSPMTC is a generator, an important task at the initial test stage was to evaluate its external characteristics. This determines the requirements for the SG control system and its topology. The external characteristic for the 4-pole topology is also presented in Figure 10, which shows that the created layout has a rather steep external characteristic.

An ideal short circuit experiment was made for the sample. In this case, the short-circuit current for the 4-pole topology was 11.7 A at a 50 Hz frequency. At low rotational speeds, the SG is able to provide a double overcurrent. The oscillogram for this mode is presented in Figure 10.



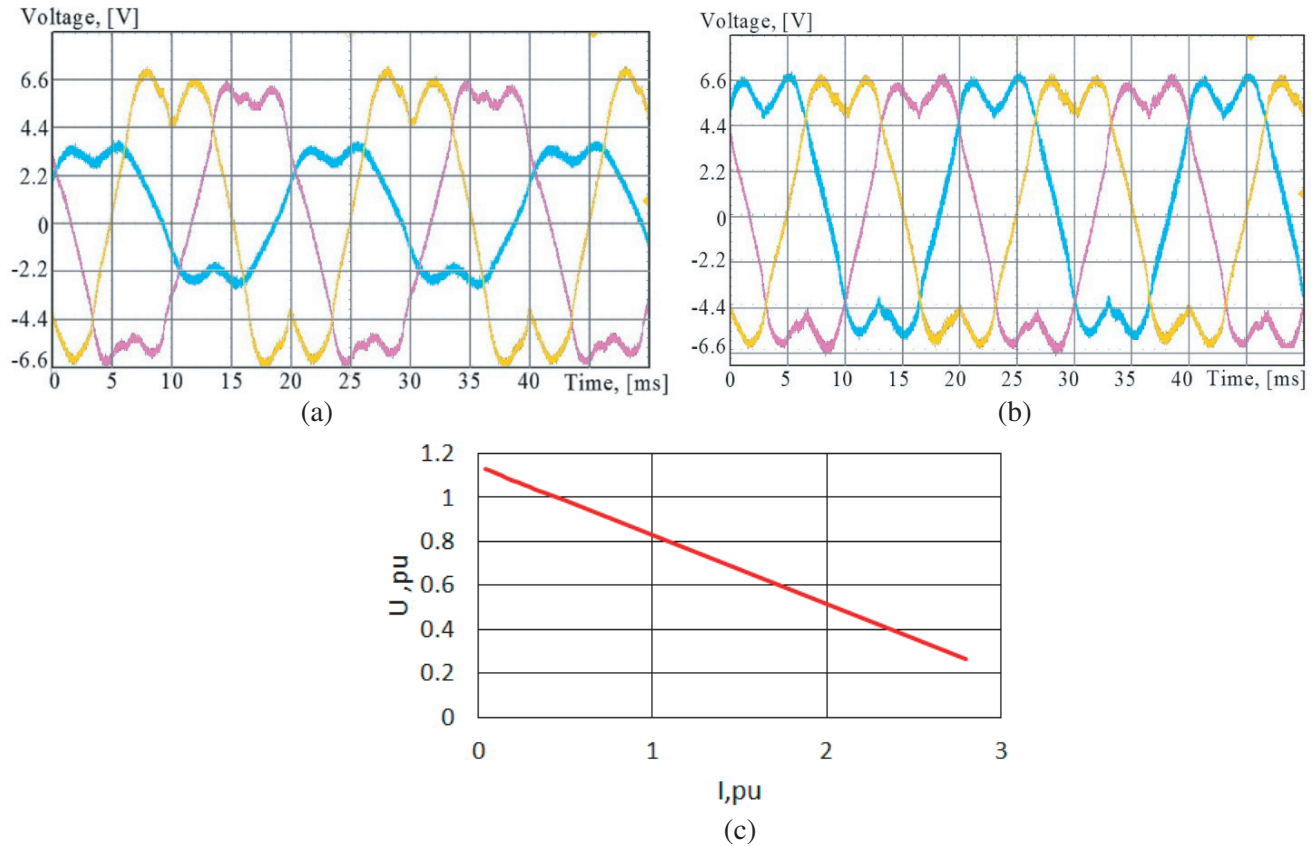


**Figure 10.** Oscillograms for the 2-pole HSPMTC in generator mode: (a) at the rated load; (b) at the double overload of one phase; (c) the external characteristic of the 4-pole HSPMTC.

Thus, the initial experimental studies have already shown that the goal has been achieved. The next stage of the research will be tests at the full frequency and power, as well as tests in the UAV.

## 5. RESULTS AND CONCLUSIONS

The article presents a new HSPMTC topology with a stator magnetic core made of amorphous alloys for prospective unmanned aerial vehicles. The global trends in this direction were considered. Conclusions about the prospects for the high-speed electrical machine development for unmanned aerial vehicles were made.

A sequence of designing HSPMTC with a stator magnetic core from amorphous alloy is proposed. This is a multidisciplinary design algorithm with optimization elements. Based on the proposed algorithm, calculations of several HSPMTC topologies were performed by using computer simulation methods, and the optimal pole number was selected. It was shown that more than one pair of poles can be effectively used in the HSPMTC with a stator core made of amorphous alloy. Consequently, the HSPMTC energy density can be increased. In addition, the analysis of the HSPMTC rotor dynamics as part of the UAV turbojet engine and the mechanical rotor strength calculations are performed.

To minimize the eddy-current losses in permanent magnets, the multicriteria optimization of the slotted zone was carried out by using genetic algorithms. In the result of this optimization, the eddy-current losses in permanent magnets were reduced by 300% in comparison with the initial variant. A cooling system of the HSPMTC was proposed, and thermal calculations were performed.

To verify the proposed design algorithm and to evaluate the efficiency of the amorphous alloy, a full-sized 5 kW experimental sample with a rotational speed of 60,000 rpm, a power density of 0.2 kg/kW and an efficiency of 96.4% was created. Initial tests of the experimental sample confirmed all theoretical

conclusions and showed that the use of amorphous alloy allows the loss reduction in the HSPMTC stator magnetic core by 400–600%.

Figure 11 shows a comparison of the designed 5 kW HSPMTC for the 1 kW turbojet TJ-50 [16] of the UAV, which demonstrates the achieved progress: the HSPM size has increased not significantly, but power is increased by 400%, while the efficiency is 96.4% taking into account the mechanical losses.



**Figure 11.** The designed 5 kW HSPMTC with the rotational speed of 60,000 rpm for UAV and the 1 kW HSPMTC for UAV by Hamilton Sundstrand [16].

The obtained results can be used to create new promising UAVs and to design electrical machines for other industrial applications. The next stage of research will be the creation of a stator magnetic core made of amorphous alloy from several magnetic cores with an axial length of 5 mm, as well as a full testing of the currently obtained prototypes for a working frequency and as part of the UAV.

## ACKNOWLEDGMENT

The work was supported by the Russian Science Foundation, project 17-79-20027.

## REFERENCES

1. Larbi, M., K. Meguenni, Y. Meddahi, and M. Litim, "Nonlinear observer and backstepping control of quadrotor unmanned aerial vehicle," *International Review of Aerospace Engineering (IREASE)*, Vol. 6, No. 5, 233–242, 2013.
2. Yun, J., S. Cho, H. C. Liu, H.-W. Lee, and J. Lee, "Design of electromagnetic field of permanent magnet generator for VTOL series-hybrid UAV," *2015 18th International Conference on Electrical Machines and Systems, ICEMS*, 83–86, 2016.
3. Besnard, J.-P., F. Biais, and M. Martinez, "Electrical rotating machines and power electronics for new aircraft equipment systems," *ICAS — Secretariat — 25th Congress of the International Council of the Aeronautical Sciences*, 1–9, 2006.
4. Chun, J., H.-C. Song, M.-G. Kang, H. B. Kang, R. Kishore, and S. Priya, "Thermo-magneto-electric generator arrays for active heat recovery system," *Sci. Rep.*, Vol. 7, No. 41383, 1–8, 2017.
5. Secttnde, R. R., R. P. Macosko, and D. S. Repas, "Integrate Engine — Generator concept for aircraft electric secondary power," National Aeronautics and Space Administration, NASA/TM X 2579, Washington, D.C., June 1972.
6. Nukki, R., A. Kilk, A. Kallaste, T. Vaimann, and K. Sr. Tiimus, "Exterior-rotor permanent magnet synchronous machine with toroidal windings for unmanned aerial vehicles," *9th International: 2014 Electric Power Quality and Supply Reliability Conference, PQ* 215–220, 2014.



7. Vavilov, V. E., F. R. Ismagilov, I. K. Khayrullin, and R. D. Karimov, "Multi-disciplinary design of high-RPM electric generator with external rotor for unmanned aerial vehicle," *International Review of Aerospace Engineering*, Vol. 9, No. 4, 123–130, 2016.
8. Upadhayay, P. and V. Patwardhan, "Magnet eddy-current losses in external rotor permanent magnet generator," *Proceedings of 2013 International Conference on Renewable Energy Research and Applications, ICRERA*, Vol. 6749911, 1068–1071, 2013.
9. Koo, V. C., Y. K. Chan, and V. Gobi, "A new unmanned aerial vehicle synthetic aperture radar for environmental monitoring," *Progress In Electromagnetics Research*, Vol. 122, 245–268, 2012.
10. Uzhegov, N., J. Pyrhonen, and S. Shirinskii, "Loss minimization in high-speed permanent magnet synchronous machines with tooth-coil windings," *IECON Proceedings (Industrial Electronics Conference)*, Vol. 6699601, 2960–2965, 2013.
11. Nagorny, A., N. Dravid, R. Jansen, and B. Kenny, "Design aspects of a high speed permanent magnet synchronous motor/generator for flywheel applications," NASA/TM-2005-213651, 1–7, 2005.
12. Chin, Y. K., "A permanent magnet synchronous motor for traction application of electric vehicle," *IEEE Int. Electric Machines and Drive Conference*, Vol. 2, 1035–1041, 2003.
13. Gieras, J. F., "High speed machines," *Advancements in Electric Machines (Power Systems)*, 81–113, 2008.
14. Borisavljevic, A., H. Polinder, and J. Ferreira, "On the speed limits of permanent-magnet machines," *IEEE Transactions on Industrial Electronics*, Vol. 57, No. 1, 220–227, 2010.
15. Vavro, J., M. Kianicová, J. Vavro, Jr., and A. Vavrová, "Modal and frequency analysis for rotor blades of turbo-jet engine TJ 100," *University Review*, Vol. 7, No. 4, 47–50, 2013.
16. Harris, M. M., A. C. Jones, and E. J. Alexande, "Miniature turbojet development at Hamilton Sundstrand the TJ-50, TJ-120 and TJ -30 turbojets," *2nd AIAA "Unmanned Unlimited" Systems, Technologies, and Operations*, Aerospac, San Diego, California, 1–9, 2003.
17. Gruzkov, S. A., et al., "Electrical equipment of aircrafts. Power supply systems for aircraft," Moscow Power Engineering Institute, Moscow, 2005.
18. Borg Bartolo, J., M. Degano, J. Espina, and C. Gerada, "Design and initial testing of a high-speed 45-kW switched reluctance drive for aerospace application," *IEEE Transactions on Industrial Electronics*, Vol. 64, No. 2, Vol. 7592921, 988–997, 2016.
19. Electric propulsion components with high power densities for aviation [Online], available: <https://nari.arc.nasa.gov/sites/default/files/attachments/Korbinian-TVFW-Aug2015.pdf>.
20. Ganev, E., "High-performance electric drives for aerospace more electric architectures," *IEEE Power Engineering Society Meeting*, 1–8, 2007.
21. Ganev, E., "Selecting the best electric machines for electrical power generation systems," *IEEE Electrification Magazine*, Vol. 2, No. 4, 13–22, 2014.
22. Wang, Z., Y. Enomoto, M. Ito, et al., "Development of a permanent magnet motor utilizing amorphous wound cores," *IEEE Trans. Magn.*, Vol. 46, No. 2, 570–573, 2010.
23. Wang, Z., Y. Enomoto, M. Ito, et al., "Development of an axial gap motor with amorphous metal cores," *IEEE Trans. Ind. Appl.*, Vol. 47, No. 3, 1293–1299, 2011.
24. Rührig, M., "Stator für eine elektrische Maschine und Verfahren zum Herstellen eines Stators für eine elektrische Maschine," Patent DE 102012207508 A1, 07.05.2012.
25. Yakupov, A., F. Ismagilov, I. Khayrullin, and V. Vavilov, "Method of designing high-speed generators for the biogas plant," *International Journal of Renewable Energy Research*, Vol. 6, No. 2, 447–454, 2016.
26. Uzhegov, N., E. Kurvinen, J. Nerg, J. T. Sopenan, and S. Shirinskii, "Multidisciplinary design process of a 6-slot 2-pole high-speed permanent-magnet synchronous machine," *IEEE Transactions on Industrial Electronics*, Vol. 63, No. 2, 784–795, 2016.
27. Zwyssig, C., J. W. Kolar, and S. D. Round, "Mega-speed drive systems: Pushing beyond 1 million RPM. Mechatronics," *IEEE/ASME Transactions*, Vol. 14, No. 5, 564–574, 2009.